Journal of Naval Architecture and Marine Engineering
June, 2016
http://dx.doi.org/10.3329/jname.v13i1.26017 http://www.banglajol.info

NUMERICAL SIMULATION OF TURBULENT BOUNDARY LAYERS OF SURFACES COVERED WITH FOUL RELEASE AND ANTIFOULING COATINGS

S. S. Kianejad[1] and N. Ansarifard[2]

[1]Center of excellent in hydrodynamics and dynamic of marine vehicles, Sharif University of Technology, Iran, *Email: kianejadsadra@gmail.com.
[2]National Centre for Maritime Engineering and Hydrodynamics, Australian Maritime College, University of Tasmania, Australia, *Email: naznin.ansarifard@utas.edu.au.

Abstract:

In order to compare the frictional resistance of three kinds of ship's hull coatings (foul release, SPC copper, SPC TBT) in the unfouled conditions, the numerical studies have been made. Simulations have been carried out for different Reynolds numbers in the range of $2.85 \times 10^6 - 5.5 \times 10^6$ *based on the plate length and flow velocity. Antifouling coatings have larger mean roughness than foul release. The results have indicated that frictional resistance coefficient of foul release test plate is lower than SPC copper and SPC TBT test plates. The total resistance obtained by computational fluid dynamics has been compared with the experimental data and its good agreement has proven the ability of CFD modeling in the calculation of fluid flow resistance, considering the coating characteristics.*

***Keywords*:** Foul release,antifouling, frictional resistance, roughness, CFD

1. Introduction

The most widely applied marine antifoulings were tributyl-tin self-polishing co-polymers (TBT-SPC), which can keep a ship surface free of fouling for 5 years, by steady releasing of the TBT toxin (Kevin, 2011). Due to the environmental side effects associated to TBT, in October 2001, the International Maritime Organization (IMO), decided to phase out the use of TBT-SPCs by 2008. There are currently two alternatives on the market also offering 5 years of satisfactory antifouling performance. The first alternative, tin-free SPC, uses the same chemical principles except TBT, instead of which it gradually leaches copper-based toxins complemented by "booster biocides". The second type, foul release coatings, works by other principles, in which instead of killing the attached marine organisms to the hull, they try to prevent the stick of the fouling by providing a low surface energy onto the organisms with great difficulty to stick. If vessels are stationary for short times, settlement can occur, but there is only weak bonding between the fouling and the foul release coating surface and so the organisms can relatively-easily be removed by the hydrodynamic forces against the surface, when the vessel is travelling fast enough. The foul release coatings described in this paper are silicone elastomers based. Experimental studies on the attachment of fouling organisms to different types of materials have shown that silicones are least prone to foul (Baier, 1970, Meyer, Baier& King, 1988). Eventually, all surfaces will foul, but experiments have also shown that the strength of attachment of the organisms on silicones is lower than other materials. Kovach and Swain towed a foil adjacent to the vessel, which was coated with a foul release system and covered by fouling, at different speeds and release at speeds up to 12 knots (Kovach & Swain, 1998). The hull condition has an important effect on the operation of marine vehicles. Skin friction has a bigger share in the total drag of most displacement ships, highlighting the impact of skin friction on some displacement ships, it has the share of about 90% of the total drag even in absence of hull foulings (Lackenby, 1962). Hence, understanding and predicting of frictional drag must be the seat of focus in this research. To find out the influence of surface roughness on the frictional drag of marine paints, some investigations was conducted by Musker (Musker, 1980–1981), Townsin et al. (Townsin, Byrne, Svensen& Milne, 1981), Granville (Granville, 1987), Medhurst (Medhurst, 1989), Grigson (Grigson, 1992) and Schultz (Schultz, 2004). These studies were concentrated on analyzing the changes in roughness and drag of the different coating systems. A substantial part of research has been dedicated to study the effects of fouling on drag, specially the calcareous macrofouling (barnacles, oysters, etc.), reviewing the marine fouling and its prevention (Anon, 1952) and focusing on the effect of plant fouling and biofilms, date back to McEntee (McEntee, 1915). Moreover, further studies to acquire higher quantify of slime films effect on drag were carried out by Picologlou et al (Picologlou, Zelver&Characklis, 1980). To detect the effect of fouling on the drag of copper-based coatings full-scale ship tests were performed by Haslbeck and Bohlander (Haslbeck&Bohlander, 1992). Schultz and Swain (Schultz &

1813-8235 (Print), 2070-8998 (Online) Received on: Dec. 2015

Swain, 1999) and Schultz (Schultz, 2000) studied the details of turbulent boundary layers developing over biofilms and filamentous algae, respectively, using laser Doppler velocimetry. As a consequence, all of these studies showed that relatively thin fouling layers can significantly increase the drag.

In some primary data from Candries et al. it can be seen that having a lower mean roughness in the unfouled condition, fouling-release systems may have slightly less frictional resistance than traditional Antifouling coatings (Candries, Atlar& Anderson, 2000). The purpose of the present numerical research is to compare the performance of foul release coatings with Antifouling coatings based on roughness. Therefore, different CFD modeling have been carried out and numerical results have been compared with available experimental data.

2. Mechanisms of Friction Drag

When a fluid flows around the outside of the body, a mechanism of energy transference between the body and fluid tends to drag it in the direction of the flow. This drag is divided into two forms of skin friction drag and form drag. Friction drag is caused by the interaction between fluid particles and surface of the body in the fluid. Boundaries between the surfaces of a body, moving through a fluid, and the layer of fluid particles in contact with the surface, cause these particles to be held in place on the surface. In this condition, the layer next to the surface may become attached to it. This is called the 'no slip condition'. In this condition, there is a linear decreasing in fluid particles' velocity from the moving body to the stationary bulk fluid till the fluid particles' velocity reaches to the bulk fluid velocity. Decrease in velocity has happened because of the forces between layers of fluid particles (intermolecular bonds) that pull each successive fluid layer and accelerate it.

When a body moves in water, the flow is laminar at the first portion of the body. As the flow continues across the body, it becomes more and more turbulent in the transition region, until it eventually becomes a turbulent flow. The length of the transition region can vary due to several factors including surface roughness, pressure and velocity fluctuations (Candries, 2001). The turbulent boundary layer is assumed to consist of two main regions: an inner region and an outer region. The inner region is composed of a viscous sub layer and a log-law region. In vicinity of the body, there is a very thin layer of fluid where turbulent fluctuations are damped, and viscosity plays an important role, the flow has a laminar manner with linearly velocity varies. The mean average velocity in this region depends upon wall shear stress, surface conditions, such as roughness, the density of the fluid, kinematic viscosity and the distance from the wall. As flow velocities increase, there is no distinct direction for particles' motion. Fluid particles exhibit velocity components in any directions and move in swirling motions such that the point velocities in the fluid flow are totally different, however the average velocity is maintained in the direction of flow. At the surface in the viscous sub layer, some stream wise vortices are created that outward ejection of these vortices causes the disorganized motion of layers in turbulent flow. As these vortices rotate and flow along the surface, they can independently translate back and forth across the surface in the cross flow direction. When the vortices in the flow collide with the surface and vortices in vicinity of the surface, an interaction between them causes the immediately ejection form the surface into the outer boundary layer. Vortices that are ejected tangle with other vortices and twist such that transient velocity vectors in the cross stream direction can become as large as those in the average flow direction. The translate laminar flow to the turbulent flow, ejection of vortices out of the laminar sub layer and disorganized flow in the outer layers of the turbulent boundary layer flow are all forms of momentum transfer and are large factors of fluid drag. Reduction of the ejection of stream wise vortices is a critical goal of drag reduction, as the drag reduction possibilities presented by this is sizable.

3. Numerical Simulation

3.1 Geometry and grid generation

A complete CFD solution requires three major steps: preprocessing, analysis of the problem by using a solver, and post processing the results. Preprocessing of the solution involves geometry creation of the model and an appropriate grid generation. In this study, preprocessing of the solution has been performed by GAMBIT software. The geometry of the plate is obtained by the use of offset table. This offset data has been imported into Gambit in the form of vertices and then 3-D model has been generated. The grid of the model and the enlarged grid near the plate surface are shown in Figs. 1 and 2. The test plate has 1.52 m length and 0.4m width. The volume domain is taken a box shape and size of box is shown in Table 1.

Table 1: Size of domain volume

Description	Dimensions (m)
Length	1.52
Width	0.4
Height	0.35

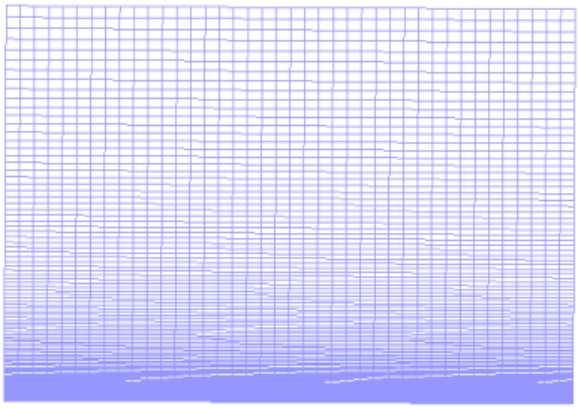

Fig. 1: Grid of velocity inlet boundary condition.

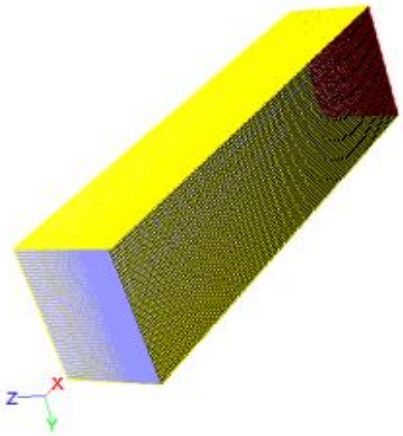

Fig. 2: Grid used for numerical simulation.

It is well-known that the grid quality of good or bad affects directly the feasibility, convergence and accuracy of numerical calculation. In this study, some principles have been abided. Firstly, the grid adopt regular grid. Secondly, the grid around the plate are denser than other grid. The grid around the plate are mostly hexagonal. Thirdly, the grid adaption approach has been applied to optimize the grid to improve the grid quality.

In order to acquire lower number of grid and subsequently lower time of simulation, grid independence study has been performed as shown in the Fig. 3. The best number of grid based on our computer performance has been considered about 800000 hexagon grid, the maximum and minimum of grid volumes are $5.48690\times10^{7}m^{3}$ and $3.65791\times10^{7}m^{3}$ respectively. The equisize skew of grid has been less than 0.8 and the grid quality has been acceptable according to the test (Ahmed, 2011, Aiguo, Ming, Xiao & Zuochao, 2012).

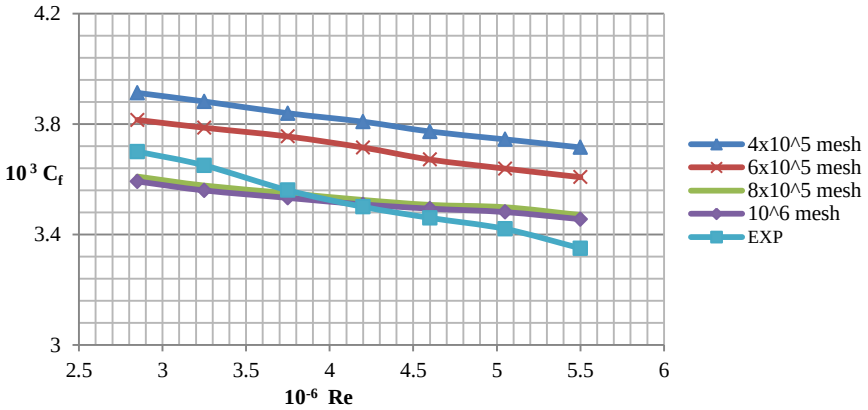

Fig. 3: Grid density on simulation result.

3.2 Governing equation

In the present study, Reynolds-averaged Navier Stokes (RANS) simulation has been conducted for plate surface. Standard k-ε turbulence models have been used in the calculations along plate surface. This study has investigated the CFD capability in solving the fluid flow around the plate surface by using commercial general-purpose software FLUENT.

Three-dimensional unsteady, incompressible and viscous turbulent flow has been considered. For incompressible flow, continuity and Navier – Stokes equation are given by:

$$\frac{\partial u_i}{\partial x_i} = 0 \quad (1)$$

$$\frac{\partial}{\partial t}(\rho u_i) + \frac{\partial}{\partial x_i}(\rho u_i u_j) = \frac{\partial}{\partial x_i}\left[\mu\left(\frac{\partial u_i}{\partial x_j} + \frac{\partial u_j}{\partial x_i}\right) - \left(\frac{2}{3}\mu\frac{\partial u_i}{\partial x_i}\right)\right] - \frac{\partial p}{\partial x_i} + \frac{\partial}{\partial x_i}\left(-p\overline{\rho u_i' u_j'}\right) \quad (2)$$

Where u_i and u_j are time-averaged velocity components (i, j=1, 2, 3), ρ is fluid density, p is pressure and μ is dynamic viscosity. In the above equation, additional terms appear that represent the effects of turbulence and $\overline{\rho u_i' u_j'}$ is called Reynolds stress. These Reynolds stresses must be modeled in order to close the equations. A turbulence model is required here in order to close the system of RANS equations.

To close the above mentioned equations, turbulence model is required to estimate the unknowns, realizable k-ϵ model has been applied. There are different types of turbulence model but every type of them could be used in limited problems. An immediate benefit of the realizable k-ϵ model is that it more accurately predicts the spreading rate of both planar and round jets. It is also likely to provide superior performance for flows involving rotation, boundary layers under strong adverse pressure gradients, separation and recirculation. The modeled transport equations for k and ϵ in the realizable k-ϵ model are (Aiguo, Ming, Bo, Xiao and Zuochao, 2012):

$$\frac{\partial}{\partial t}(\rho k) + \frac{\partial}{\partial x_j}(\rho k x_j) = \frac{\partial}{\partial x_j}\left[(\mu + \frac{\mu_t}{\sigma_k})\frac{\partial k}{\partial x_j}\right] + G_k + G_b - \rho\epsilon - Y_M + S_k \quad (3)$$

$$\frac{\partial}{\partial t}(\rho \epsilon) + \frac{\partial}{\partial x_j}(\rho \epsilon u_j) = \frac{\partial}{\partial x_j}\left[(\mu + \frac{\mu_t}{\sigma_\epsilon})\frac{\partial \epsilon}{\partial x_j}\right] + \rho C_1 S_\epsilon - \rho C_2 \frac{\epsilon^2}{K + \sqrt{\nu\epsilon}} - S_\epsilon \quad (4)$$

$$C_1 = Max\left[0.43, \frac{\eta}{\eta+5}\right], \quad \eta = S\frac{K}{\epsilon}, \quad S = \sqrt{2S_{ij}S_{ij}} \quad (5)$$

In these equations, G_k represents the generation of turbulence kinetic energy due to the mean velocity gradients, G_b is the generation of turbulence kinetic energy, due to buoyancy. Y_M represents the contribution of the fluctuating dilatation incompressible turbulence to the overall dissipation rate. C_2 and $C_{1\epsilon}$ are constants. σ_k and σ_ϵ are the turbulent Prandtl numbers for k and ϵ, respectively. S_k and S_ϵ are user-defined source terms.

Three-dimensional RANS equation of viscous and incompressible flows have been solved directly, and the differential equations have been discretized by finite volume (FV) approach. Segregated method has been used to solve the control equations after these equations have been discretized. k-ϵ turbulence model has been adopted based on its above-mentioned advantages. To deal with coupling between velocity and pressure, SIMPLEC (Semi-implicit for pressure-linked equations consistent) algorithm and stand scheme for pressure discretization have been used. UPWIND scheme has been adopted to keep the mass conservative. The convergence criterion of the residuals has been about 10^{-4}.

3.3 Boundary condition

The boundary conditions have been treated as follows (Fig. 4):

1) The inlet boundary condition upstream has been taken as velocity-inlet.
2) The outlet boundary condition upstream has been taken as pressure-outlet.
3) Among the span wise and top of the flow field, the flow has not been constrained, in order to avoid other disturbance of the flow field, the boundary along the span wise and top of the computational flow field has been set as in a symmetry condition.
4) The bottom smooth wall has been set as in no-slip boundary condition (Ahmed, 2011, Aiguo, Ming, Xiao &Zuochao, 2012).

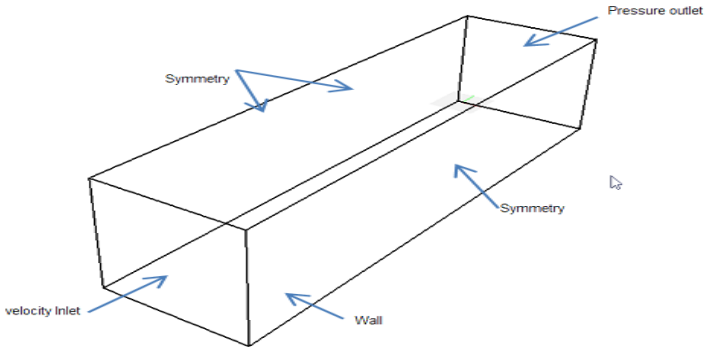

Fig. 4: Test plate domain with boundaries applied.

3.4 Wall roughness effect

Experiments indicate that mean velocity distribution near the rough walls, when plotted in the usual semi-logarithmic scale, has the same slope ($\frac{1}{k}$) but a different intercept (additive constant B in the log-law). Thus, the law-of-the-wall for mean velocity, modified for roughness, has the form below (Blocken, Stathopoulos &Carmeliet, 2007):

$$\frac{u_p u^*}{\frac{\tau_w}{\rho}} = \frac{1}{k} ln\,(E\frac{\rho u_p u^*}{\mu}) - \Delta B \quad (6)$$

$$u^* = C_\mu^{1/4} K^{1/2} \quad (7)$$

$$\Delta B = \frac{1}{k} ln\, f_r \quad (8)$$

$$k_s^+ = \rho k_s u^*/\mu \quad (9)$$

Where f_r is a function of roughness that quantifies the shift of the intercept due to roughness effects.ΔB (roughness function) depends, in general, on the type (uniform sand, rivets, threads, ribs, mesh-wire, etc.) and size of the roughness. There is no universal roughness function valid for all types of roughness. For a sand-grain roughness and similar types of uniform roughness elements, however, ΔB has been found to be well-correlated with the non-dimensional roughness height (k_s^+), where k_s is the physical roughness heightand u^* is wall-function friction velocity, τ_w is wall shear stress, ρ is fluid density, κ is von Karman constant. E is empirical constant for a smooth wall in wall function, μ is dynamic molecular viscosity, Cμ is constant in the k-ε model and k is turbulent kinetic energy. Analyses of experimental data show that the roughness function is not a single function of k_s^+ but takes different forms depending on the k_s^+ value. It has been observed that there are three distinct regimes:

1) hydrodynamically smooth $k_s^+ \leq 2.25$
2) transitional $2.25 < k_s^+ \leq 90$
3) fully rough $k_s^+ > 90$

According to the data, roughness effects are negligible in the hydrodynamically smooth regime, but become increasingly important in the transitional regime and take full effect in the fully rough regime. The whole roughness regime is subdivided into three regimes, and the formulas proposed by Cebeci and Bradshaw based on Nikuradse's data are adopted to compute ΔB for each regime (Cebeci, T., and Bradshaw, P. (1977).
For the hydrodynamically smooth regime $k_s^+ \leq 2.25$:

$$\Delta B = 0 \quad (10)$$

For the transitional regime $2.25 < k_s^+ \leq 90$:

$$\Delta B = \frac{1}{k} ln\,[\frac{k_s^+ - 2.25}{87.75} + c_s k_s^+] \times sin\{0.4258\,(ln\, k_s^+ - 0.811)\} \quad (11)$$

Where c_s is the constant of roughness which is depended on the roughness type. In this simulation c_s = 0.5.

In the fully rough regime $k_s^+ > 90$:

$$\Delta B = \frac{1}{k} ln\,(1 + c_s k_s^+) \quad (12)$$

In this numerical simulation k_s^+ for foul release (k_s=66μm), SPC copper (k_s=97μm), SPC TBT (k_s=127μm)are 22, 32 and 42 respectively.

3.5 Resistance calculation

Drag is the component of hydrodynamic force opposite to the direction of motion. Drag has been countered by thrust which is provided by a propelling mechanism. Drag depends on velocity as follow:

$$c_f = \frac{D}{.5 \times \rho \times A \times V^2} \quad (13)$$

In this equation D, ρ, A and V are drag, density, wetted surface and velocity respectively. The total resistance of the plate can be calculated by this equation.The CFD simulations are carried out for Reynolds numbers ranging from $(2.85 - 5.5) \times 10^6$.The drag measurement on the plate has been recorded after every 400 iterations. It can be observed that turbulence models predict total resistance of plate quite accurately in the Tables 2, 3 and 4 and Figs. 5, 6 and 7. In each figure, the CFD results have been compared with experimental (EXP) results (Schultz, 2004).

Table 2:Resistance coefficient result of the foul release coating.

Reynolds ($\times 10^6$)	Velocity (m/s)	Resistance coefficient ($\times 10^{-3}$)
2.85	1.9	3.6096
3.25	2.1	3.5771
3.75	2.5	3.5495
4.2	2.8	3.5249
4.6	3	3.5072
5.05	3.3	3.4986
5.5	3.6	3.4704

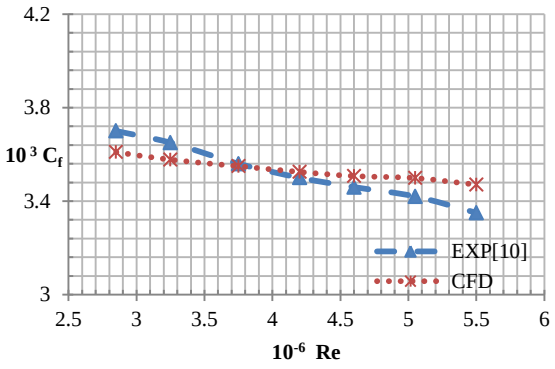

Fig. 5: Frictional resistance coefficient versus Reynolds number for foul release test plate.

Table 3: Resistance coefficient result of SPC copper paint.

Reynolds ($\times 10^6$)	Velocity (m/s)	Resistance coefficient ($\times 10^{-3}$)
2.85	1.9	3.7769
3.25	2.1	3.7643
3.75	2.5	3.7565
4.2	2.8	3.7419
4.6	3	3.7394
5.05	3.3	3.7327
5.5	3.6	3.7268

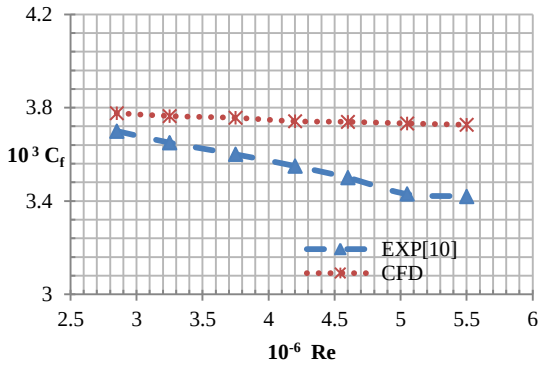

Fig. 6: Frictional resistance coefficient versus Reynolds number for SPC copper test plate

Table 4: Resistance coefficient result of SPC TBTpaint.

Reynolds ($\times 10^6$)	Velocity (m/s)	Resistance coefficient ($\times 10^{-3}$)
2.85	1.9	3.8712
3.25	2.1	3.8685
3.75	2.5	3.8628
4.2	2.8	3.8634
4.6	3	3.8726
5.05	3.3	3.8779
5.5	3.6	3.8832

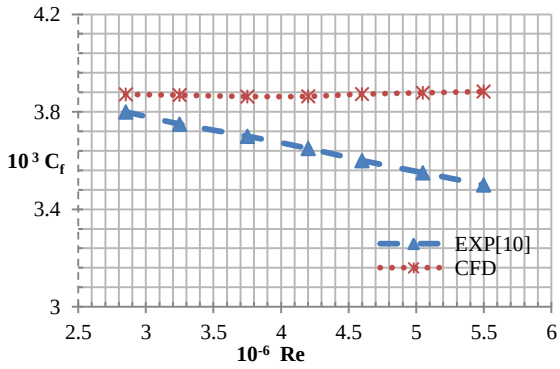

Fig. 7: Frictional resistance coefficient versus Reynolds number for TBT test plate.

The frictional resistance results are presented for the test plate. At the lowest Reynolds number, the SPC copper and SPC TBT test plates showed an increase in C_f compared to the foul release test plate. At the highest Reynolds number, silicone fouling release surfaces tended to have lower frictional resistance than the other antifouling surfaces over the entire range of tested Reynolds numbers. The lower drag can be explained by the fact that the silicone surfaces were smoother than the other Antifouling surfaces. In other words, the roughness height has a direct impact on frictional resistance because decrease fluid velocity near the plate and increase turbulence intensity and subsequently resistance of plate. Wall roughness effects in hydro-dynamically smooth and transitional regions have been simulated accurately, but fully rough regime boundary condition could not be simulated when the height of roughness increased. On the other hand, with increase in the velocity and Reynolds number the accuracy of simulation has been diminished. Fig. 8 shows the difference between three test plates resistance coefficients from numerical simulation with the experimental results of Schultz (Schultz, 2004).

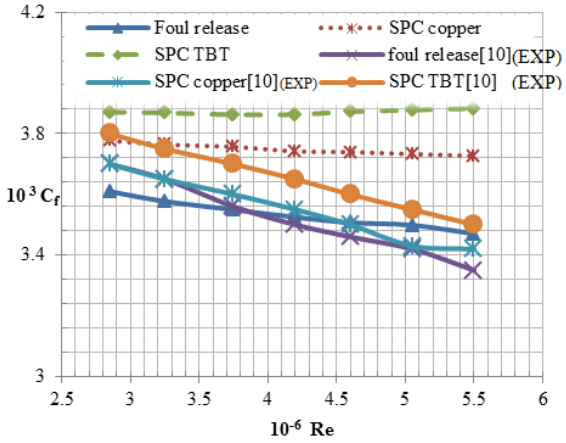

Fig. 8: Frictional resistance coefficient versus Reynolds number.

3.6 Analysis of velocity profile

Figs. 9 and 10 show the velocity profile in the boundary layer on the test plate. The effect of different types of coating on the size of boundary layer is not striking. Velocity gradient directly impacts on wall friction. If velocity gradient in boundary layer increases, the friction of wall would grow up. Velocity in first grid adjacent to foul release test plate has greater magnitude than other test plates therefore velocity gradient on foul release is lower than SPC copper and SPC TBT test plates. As well as this, the wall friction of foul release is lower than SPC copper and SPC TBT test plate.

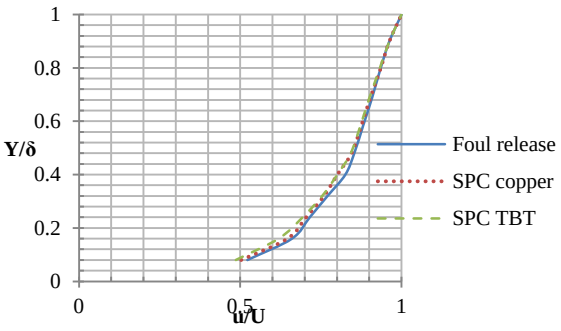

Fig. 9: Velocity profile in boundary layer (35 cm from inlet).

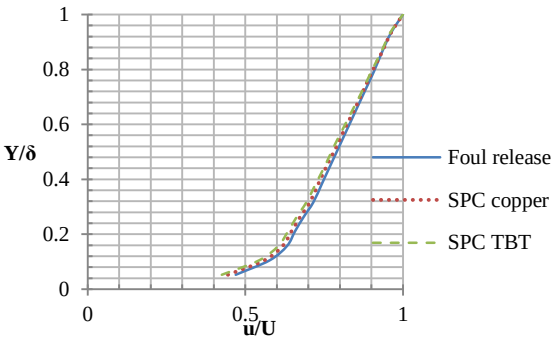

Fig. 10: Velocity profile in boundary layer (121 cm from inlet).

3.7 Analysis of shear stress

If the average velocity in the flow field reaches 3.62 m/s, the Reynolds number exceeds the critical value, after small part from leading edge, including laminar and transition regions, flow becomes turbulent (Wu, and Moin, 2009). The amount of sheer stress in the flow direction (leading edge (0 mm) until tail-end edge (1520 mm)) on foul release, SPC copper and SPC TBT test plates are shown in Fig. 11. According to the figure, the sheer stress on foul release test plate is about 18.3 pa – 73.3 pa, sheer stress on SPC copper test plate is about 17.3 pa – 86.3 pa and sheer stress on SPC TBT test plate is about 14 pa – 93.6 pa.

3.8 Analysis of turbulence intensity

The turbulence intensity can directly affect the flow state and influence the wall friction. The amount of turbulence intensity over foul release, SPC copper and SPC TBT test plates (leading edge (0 mm) until tail-end edge (1520 mm)) are shown in Fig. 12. The turbulence intensity in the inlet region of the flow field is larger than other regions and the intensity near the SPC TBT test plate is larger than near the foul release test plate and SPC copper test plate. The turbulence intensity on foul release test plate is about 15.5 % – 38.7%, turbulence

intensity on SPC copper test plate is about 18.7% – 41.6% and turbulence intensity on SPC TBT test plate is about 20.1 % – 44.7%.

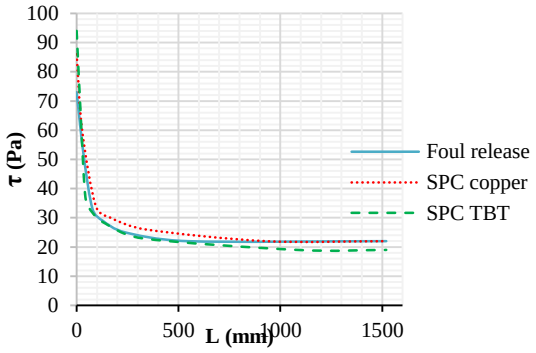

Fig. 11: Amount of X -wall sheer stress on test plate (v = 3.62 m/s).

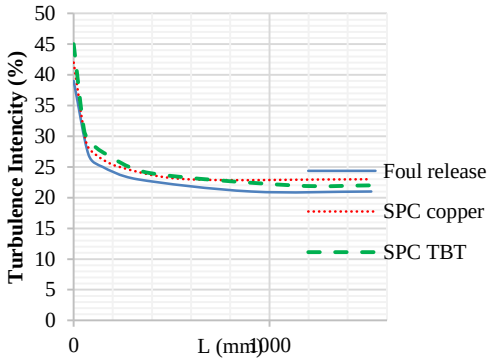

Fig. 12: Amount of turbulence intensity on test plate (v = 3.62 m/s).

3.9 Roughness effect on ship

Effect of different coatings on ship could be obtained from model simulation and by contribution of Granville similarity (Granville, 1958, 1987). First step, C_f of smooth surface has been computed by Equation (14) and has been plotted as a function of Log 10 (Re). The rough surface frictional resistance coefficient for a known roughness function has been determined by displacing the smooth friction line by a distance ΔU^+/ (ln(10)/k) in the positive Log 10 (Re) direction which ΔU^+ obtain by Equation (17). The next step L+ of model test has been calculated by Equation (19) and the diagram of L+ as function of Reynolds Number has been plotted. In the final step the diagram of L+ has been transported by Log (Lship/Lmodel) in the positive Log 10 (Re) direction, the intersection of this diagram and rough surface diagram has been identified C_f for the rough plate. In this study, the effect of foul release, SPC copper and SPC TBT coatings on a ship with 100 meters length has been predicted and the calculation procedures of C_f are shown in Figs. 13, 14 and 15. C_f for a ship with 100 meter length and 5.25 m/s velocity and foul release, SPC copper and SPC TBT coatings have been estimated as 0.0018, 0.002 and 0.0021 respectively.

$$C_f = \frac{0.075}{(log_{10}^{Re}-2)^2} \quad (14)$$

$$U_\tau = \sqrt{\frac{\tau_W}{\rho}} \quad (15)$$

$$U^+ = \frac{U}{U_\tau} \quad (16)$$

$$\Delta U^+ = U^+_{smooth} - U^+_{rough} \quad (17)$$

$$L^+ = \frac{L\,U_\tau}{\upsilon} \quad (18)$$

$$L^+ = Re_L\left(\sqrt{\frac{C_F}{2}}\left(1-\frac{1}{K}\sqrt{\frac{C_F}{2}}\right)\right) \quad (19)$$

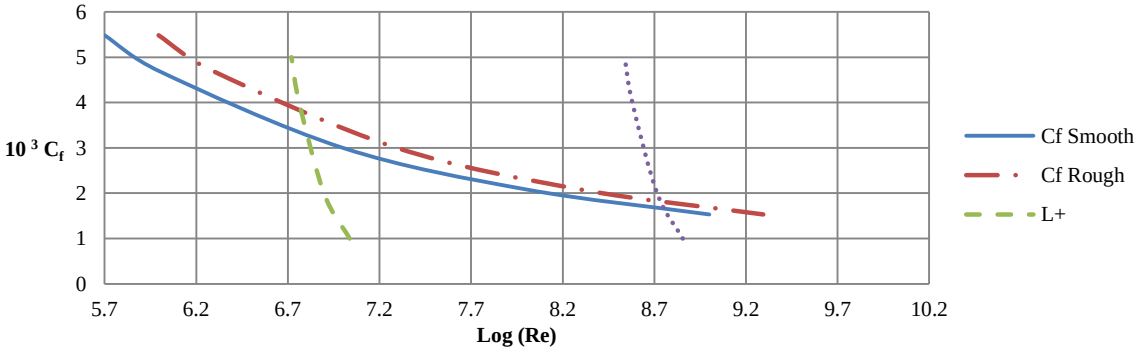

Fig. 13: Scaled-up $C_{F\ Rough}$ from $C_{F\ Smooth}$ for foul release coatings

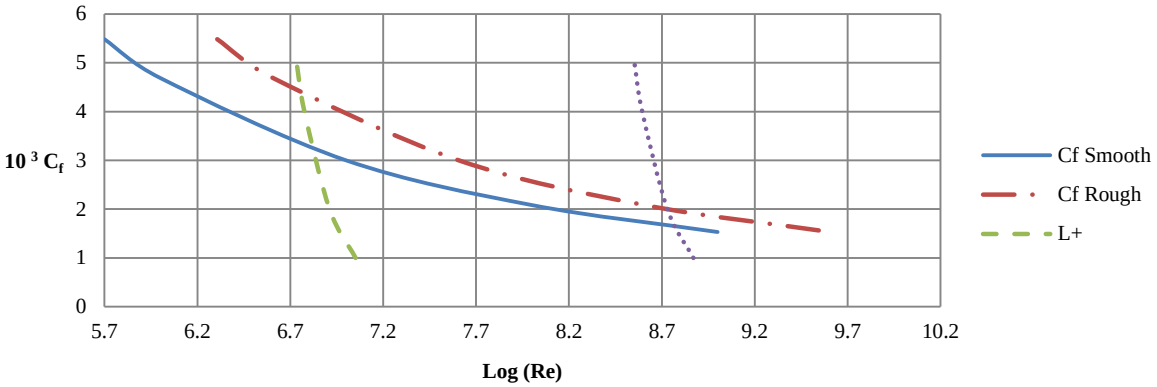

Fig. 14: Scaled-up $C_{F\ Rough}$ from $C_{F\ Smooth}$ for SPC copper coatings

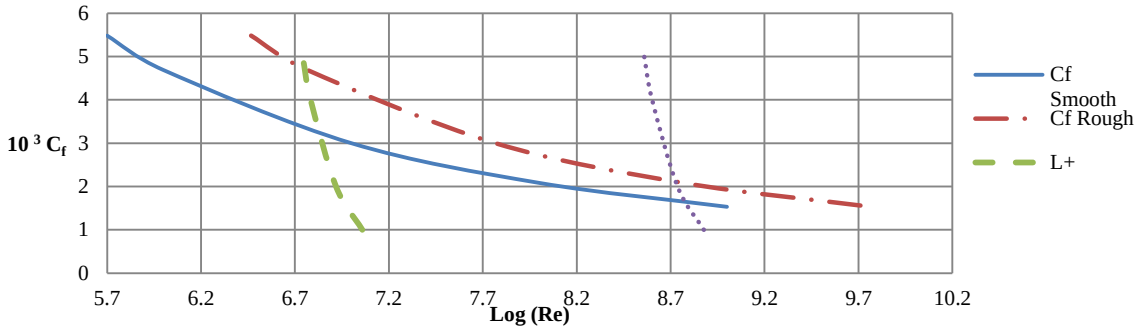

Fig. 15: Scaled-up $C_{F\ Rough}$ from $C_{F\ Smooth}$ for SPC TBT coatings

4. Conclusions

Total resistances of foul release test plate, SPC copper test plate and SPC TBT test plate have been evaluated in this study. GAMBIT software has been used for geometry creation and generation of grid. Hydrodynamic simulations have been carried out by Commercial CFD software FLUENT for Reynolds number in the range of $2.85 \times 10^6 - 5.5 \times 10^6$ based on the plate length and flow velocity. The total resistance obtained by computational fluid dynamics has been compared with the experimental data and good agreement in results has been gained. The frictional resistance has a direct relation with the height of roughness of different coatings,foul release coating based on silicon makes the lowest roughness. According to the simulations, the frictional resistance coefficient of foul release test plate is lower than SPC copper and SPC TBT test plates. The effect of foul release on fluid is lower than other coatings; the velocity of fluid near the foul release test plate is higher than other test plates, therefore turbulence intensity, velocity gradient and sheer stress have been decreased in comparison to SPC copper and SPC TBT.

References

Ahmed, Y.M. (2011): Numerical simulation for the free surface flow around a complex ship hull form at different Froude numbers, Alexandria Engineering Journal, 50, 229–235.
http://dx.doi.org/10.1016/j.aej.2011.01.017
Aiguo, S., Ming, W., Bo, Y., Xiao, W., Zuochao, W. (2012): Resistance Calculation and Motions Simulation for Free Surface Ship Based on CFD", Procedia Engineering, 31 68-74.
http://dx.doi.org/10.1016/j.proeng.2012.01.992
Anon, (1952): Marine Fouling and Its Prevention, Woods Hole Oceanographic Institution.
Baier, R. E. (1970): Surface Properties Influencing Biological Adhesion, in Adhesion in Biological Systems, R. S. Manly, ed., Academic, New York, pp. 15–48.http://dx.doi.org/10.1016/B978-0-12-469050-9.50007-7
Blocken, B., Stathopoulos, T., Carmeliet, J. (2007): CFD simulation of the atmospheric boundary layer:-wall function problems, Atmospheric Environment 41(2): 238-252.
http://dx.doi.org/10.1016/j.atmosenv.2006.08.019
Candries, M., Atlar, M., and Anderson, C. D. (2000): Considering the Use of Alternative Antifoulings: the Advantages of Foul-Release Systems, Proceedings ENSUS 2000, Newcastle, UK, pp. 88 –95.

Candries, M. (2001): Drag, Boundary layer and Roughness Characteristics of Marine Surfaces Coated with Antifoulings (Ph.D. thesis), Department of Marine Technology, University of Newcastle-upon-Tyne, UK.
Cebeci, T., and Bradshaw, P. (1977): Momentum Transfer in Boundary Layers, Hemisphere Publishing Corporation, New York.
Granville PS.(1958): The frictional resistance and turbulent boundary layer of rough surfaces, Journal Ship Research, 2:52 – 74.
Granville, P. S.(1987): Three Indirect Methods for the Drag Characterization of Arbitrarily Rough Surfaces on Flat Plates, Journal Ship Research, 31, pp. 70–77.
Grigson, C. W. B.(1992): Drag Losses of New Ships Caused by Hull Finish, Journal Ship Research, 36, pp. 182–196.
Haslbeck, E. G., and Bohlander, G. (1992): Microbial Biofilm Effects on Drag—Lab and Field, Proceedings of SNAME Ship Production Symposium, 1992.
Lackenby, H. (1962): Resistance of Ships, With Special Reference to Skin Friction and Hull Surface Condition, Proceedings of the Institution of Mechanical Engineers, 176, pp. 981–1014.
http://dx.doi.org/10.1243/PIME_PROC_1962_176_077_02
Meyer, A. E., Baier, R. E., and King, R. W. (1988): Initial Fouling of Nontoxic Coatings in Fresh, Brackish and Sea Water, Canadian Journal of Chemical Engineering, 66, pp.55–62.http://dx.doi.org/10.1002/cjce.5450660108
Kevin P. L., (2011): Using a Ship's Propeller for Hull Condition Monitoring, ASNE Intelligent Ships Symposium IX, Philadelphia, PA, USA.
Kovach, B. S., and Swain, G. W. (1998): A Boat Mounted Foil to Measure the Drag Properties of Antifouling Coatings Applied to Static Immersion Panels, Proc. International Symposium on Seawater Drag Reduction, Newport, Rhode Island, pp. 169–173.
McEntee, W. (1915): Variation of Frictional Resistance of Ships With Condition of Wetted Surface, Trans. SNAME, 24, pp. 37– 42.
Medhurst, J. S. (1989): The Systematic Measurement and Correlation of the Frictional Resistance and Topography of Ship Hull Coatings, With Particular Reference to Ablative Antifoulings, Ph.D. Thesis, University of Newcastle-upon-Tyne, Newcastle, UK.
Musker, A. J. (1980–1981): Universal Roughness Functions for Naturally-Occurring Surfaces, Transactions of the Canadian Society for Mechanical Engineering, 1, pp. 1– 6.
Picologlou, B. F., Zelver, N., and Characklis, W. G. (1980): Biofilm Growth and Hydraulic Performance, Journal of the Hydraulics Division, American Society of Civil Engineers, HY5, pp.733–746.
Schultz, M. P. (2004): Frictional Resistance of Antifouling Coating Systems, ASME Journal of Fluids Engineering, 126, pp. 1039–1047.http://dx.doi.org/10.1115/1.1845552
Schultz, M. P. (2000): Turbulent Boundary Layers on Surfaces Covered With Filamentous Algae, ASME Journal of Fluids Engineering, 122, pp. 357–363.http://dx.doi.org/10.1115/1.483265
Schultz, M. P., Swain, G. W. (1999): The Effect of Biofilms on Turbulent Boundary Layers, ASME Journal of Fluids Engineering, 121, pp. 733–746.http://dx.doi.org/10.1115/1.2822009
Townsin, R. L., Byrne, D., Svensen, T. E., and Milne, A. (1981): Estimating the Technical and Economic Penalties of Hull and Propeller Roughness, Trans. SNAME, 89, pp. 295–318.
Wu, X., Moin, P. (2009): Direct numerical simulation of turbulence in a nominally zero pressure-gradient flat-plate boundary layer, Journal Fluid Mechanics, 630, 5–41.http://dx.doi.org/10.1017/S0022112009006624